Volume 49
Number 29
7 August 2025
Pages 12455–12886

NJC

New Journal of Chemistry

A journal for new directions in chemistry

rsc.li/njc

ISSN 1144-0546

ROYAL SOCIETY OF CHEMISTRY

PAPER

Wim Klopper, Stefan Bräse *et al.*

Blue to yellow-emitting neutral Cu(I) complexes with μ-bridging 1,2,4-triazole: synthesis, photophysical characterization and DFT calculations

cnrs

NJC

ROYAL SOCIETY OF CHEMISTRY

PAPER

View Article Online
View Journal | View Issue

Cite this: *New J. Chem.*, 2025, **49**, 12468

Blue to yellow-emitting neutral Cu(I) complexes with μ-bridging 1,2,4-triazole: synthesis, photophysical characterization and DFT calculations†

Valentina Ferraro, ‡[a] Xuemin Gan, ‡[a] Florian R. Rehak, [b] Philipp Ralle, [c] Martin Nieger, [d] Andreas Steffen, [c] Wim Klopper *[be] and Stefan Bräse *[af]

Received 8th March 2025,
Accepted 9th April 2025

DOI: 10.1039/d5nj01056j

rsc.li/njc

A series of Cu(I) complexes having 1,2,4-triazole as bridging ligand and aminophosphanes as chelating [NP]-donors were successfully isolated and spectroscopically characterized. The structure of the Cu(I) derivatives was ascertained through single-crystal X-ray diffraction confirming the formation of dimers. The Cu(I) species were characterized by absorptions below 400 nm, with no metal-to-ligand charge transfer (MLCT) band observable in the visible region of the spectrum. Upon excitation with UV light, the Cu(I) complexes exhibited appreciable blue to yellow emissions with lifetimes in the 2–9 μs range and photoluminescent quantum yields up to 0.42. The photophysical properties were investigated in the solid state and polymeric matrix both at room temperature and 77 K. The increased lifetimes τ at low temperatures and the two orders of magnitude different radiative decay constants k_r at 297 and 77 K suggest the presence of two different decay channels (fluorescence and phosphorescence), thus indicating thermally activated delayed fluorescence (TADF). The experimental data were supported by computational studies, further confirming the presence of TADF properties.

Introduction

1,2,4-Triazole and its derivatives have gained particular attention as ligands for transition metal elements since they combine the coordination geometry of both pyrazoles and imidazoles, and they can act as bridging ligands between two metal centres.[1,2] As highlighted in Fig. 1a, 1,2,4-triazole is an electron-rich heterocycle containing one acidic pyrrole-like NH group in position 1 and a basic pyridine-like nitrogen in position 2. While the NH group can easily donate its proton, the basic pyridine-like nitrogen can accept protons even more readily; hence, the μ-bridging coordination mode is usually found for many anionic triazoles, leaving the nitrogen atom in 4-position unsubstituted (see Fig. 1b).[3] In this bridging mode, the two metal ions are located at distances of about 400 pm, and the M–N–N angles are close to 126°. This peculiar feature and the relatively easy synthesis make them suitable for designing new transition metal complexes.[1]

On the other hand, NP-ligands such as aminophosphanes are used with Cu(I) halides to prepare luminescent derivatives due to their tuneable electronic and steric properties.[4–6] For instance, Yersin *et al.* described the use of 2-diphenylphosphanyl-*N*,*N*-dimethylaniline and diphenyl-(2-pyrrolidin-1-ylphenyl)phosphine for the synthesis of blue- and green-emitting Cu(I) dimers exhibiting thermally activated delayed fluorescence (TADF) to be applied

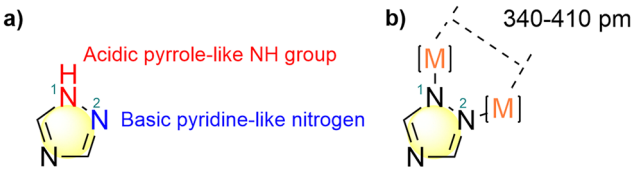

Fig. 1 (a) Structure of 1,2,4-triazole emphasizing the nitrogen atoms in position 1 and 2; (b) bridging coordination mode of 1,2,4-triazole.

[a] *Institute for Organic Chemistry (IOC), Karlsruhe Institute of Technology (KIT), Kaiserstrasse 12, 76131 Karlsruhe, Germany. E-mail: braese@kit.edu*
[b] *Institute of Physical Chemistry (IPC), Karlsruhe Institute of Technology (KIT), Kaiserstrasse 12, 76131 Karlsruhe, Germany. E-mail: klopper@kit.edu*
[c] *Department of Chemistry and Chemical Biology, TU Dortmund University, Otto-Hahn-Strasse 6, 44227 Dortmund, Germany*
[d] *Department of Chemistry, University of Helsinki, A.I. Virtasen Aukio 1, P.O. Box 55, FI 00014 Helsinki, Finland*
[e] *Institute of Nanotechnology (INT), Karlsruhe Institute of Technology (KIT), Kaiserstrasse 12, 76131 Karlsruhe, Germany*
[f] *Institute of Biological and Chemical Systems-Functional Molecular Systems (IBCS-FMS), Karlsruhe Institute of Technology (KIT), Kaiserstrasse 12, 76131 Karlsruhe, Germany*

† Electronic supplementary information (ESI) available. CCDC 2380060–2380064. See DOI: https://doi.org/10.1039/d5nj01056j

‡ Valentina Ferraro and Xuemin Gan equally contributed to this work.

for the preparation of organic light-emitting diodes (OLEDs).[7,8] Similarly, the use of bulkier tridentate NPP- and tetradentate PNNP-ligands afforded emissive Cu(I) complexes characterized by long-lived excited states lifetimes and high quantum yields due to the low degree of reorganization between the ground and the excited state.[9–11] Other types of NP ligands instead of aminophosphane are constituted by 2-diphenylphosphinopyridine and its derivatives.[12–19] This type of chelating [NP]-donor ligands was deeply investigated by our research group in combination with Cu(I) halides for the preparation of derivatives to be employed for OLED applications.[20–24]

Given our interest in the preparation of Cu(I) complexes exhibiting TADF,[6,20–25] we deemed it interesting to investigate the effect of a bridging 1,2,4-triazole ligand in the photophysical properties of the corresponding Cu(I) dimers. Herein, we report the synthesis and characterization of a series of luminescent neutral Cu(I) complexes having bridging 1,2,4-triazoles and aminophosphanes as coordinated [NP]-donor ligands. The molecular structure of the derivatives was ascertained through single-crystal X-ray diffraction. The photophysical properties were investigated at room temperature and 77 K both in the solid state and in a poly(methyl)methacrylate (PMMA) matrix, and supported by density functional theory (DFT) and time-dependent DFT (TD-DFT) calculations confirming the presence of TADF properties.

Results and discussion

Synthesis and characterization of the complexes

The NP-ligands were synthesized by first functionalizing the amino group with methyl iodide or 1,4-dibromobutane, as observable in Scheme 1. Then the phosphine group was introduced by phosphorylation reaction with the corresponding chloro(diaryl)-phosphine in the presence of *n*-butyllithium (2.5 M in hexane). 2-(Diphenylphosphanyl)-*N*,*N*-dimethylpyridin-3-amine (**N$_{py}$P**) was synthesized as previously reported by Lu *et al.* employing diphenylphosphine, palladium(II) acetate and potassium acetate.[4] For the preparation of the corresponding Cu(I) complexes, 1,2,4-triazole was deprotonated with ^{t}BuOK in dry dichloromethane (DCM) under Ar atmosphere, and the mixture was added to a solution containing CuCl and the NP-ligand in dry DCM. After filtering off the KCl, the Cu(I) complexes were isolated in good yields (43–68%) as pale solids. The derivatives were stable as solids under air, but rapidly oxidated once dissolved in chlorinated solvents, *e.g.* $CDCl_3$.

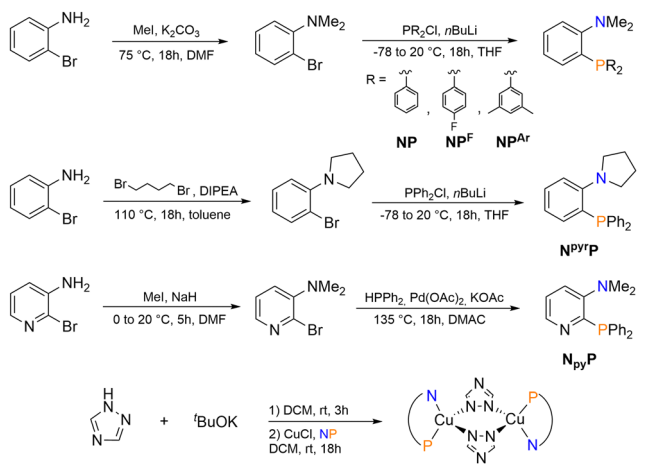

Scheme 1 Synthesis of the NP-ligands and the corresponding Cu(I) complexes.

Crystals suitable for X-ray diffraction were obtained by slow diffusion of diethyl ether vapours in dichloromethane solutions under argon atmosphere. Crystallographic and refinement data are collected in the ESI† (Tables S1 and S3), together with selected distances and angles (Tables S2 and S4–S6, ESI†). The X-ray structures are collected in Fig. 2.

In all the complexes, two Cu(I) atoms are bridged with the two anionic 1,2,4-triazole ligands, forming a six-membered ring structure. Both the metal centres adopt a distorted tetrahedral geometry, coordinated by one N of μ-trz1 and one of μ-trz2, and the respective chelating NP-ligand. **[Cu(μ-trz)(NP^{Ar})]$_2$** crystallized with a molecule of water and dichloromethane in the asymmetric unit. Except for **[Cu(μ-trz)(NP^{Ar})]$_2$**, the tetrahedral environment around the metal centre is highly distorted, with the angles N–Cu1–P1 and N–Cu1–N^{trz} respectively around 75–80° and 127–132°. Two different symmetric arrangements were found for the investigated substances: complexes **[Cu(μ-trz)(NP)]$_2$**, **[Cu(μ-trz)(NP^F)]$_2$**, **[Cu(μ-trz)(N^{pyr}P)]$_2$** and **[Cu(μ-trz)(N$_{py}$P)]$_2$** show C_i symmetry, with a centre of inversion at the midpoint of the Cu–N bond of the six-membered moiety, while complex **[Cu(μ-trz)(NP^{Ar})]$_2$** displays C_s symmetry. The six-membered ring is formed by the four nitrogen atoms of the two anionic 1,2,4-triazole ligands and the two coplanar Cu(I) atoms. The central hexagonal core is distorted, being the N–Cu1–N angle in the range of 109–111°, instead of the expected 120°. On the other hand, all the other angles of the hexagon are comprised between 123° and 127°. The distortion is mainly induced by the more rigid **NP^{Ar}** ligand. Similarly to what is observed in other binuclear [Cu(μ-X)(NP)]$_2$ complexes (X = Cl, Br, I),[7] the N–Cu–P bite angles are comprised between 121.85 and 131.89°, whereas the corresponding Cu–P and Cu–N bond lengths are around 2.18 Å and 1.98 Å, respectively.

The μ-bridging mode of the anionic 1,2,4-triazole leads to a Cu–Cu distance between 3.60 and 3.69 Å for all the measured complexes. This distance is significantly longer than the sum of the van der Waals radii (2.80 Å), ruling out any possible cuprophilic interaction.[26] The highest value was measured with **N$_{py}$P** as chelating ligand, but the Cu–Cu distance remained almost constant for all the other NP ligands, suggesting a negligible influence of the alkyl *N*-substituents.

Differently from previously reported binuclear butterfly-shaped Cu(I) complexes having chelating NP-ligands,[7] the interplanar distance between the centroids originating from the six-membered rings is found between 9.23 and 11.91 Å for **[Cu(μ-trz)(NP)]$_2$**, **[Cu(μ-trz)(NP^F)]$_2$**, **[Cu(μ-trz)(N^{pyr}P)]$_2$** and **[Cu(μ-trz)(NP^{Ar})]$_2$**, suggesting the absence of intermolecular interactions. Instead, complex **[Cu(μ-trz)(N$_{py}$P)]$_2$** exhibits a highly distorted and asymmetric configuration and disordered molecular packing arrangement. The different molecular packing of **[Cu(μ-trz)(NP)]$_2$** and **[Cu(μ-trz)(N$_{py}$P)]$_2$** is observable in Fig. S1 (ESI†).

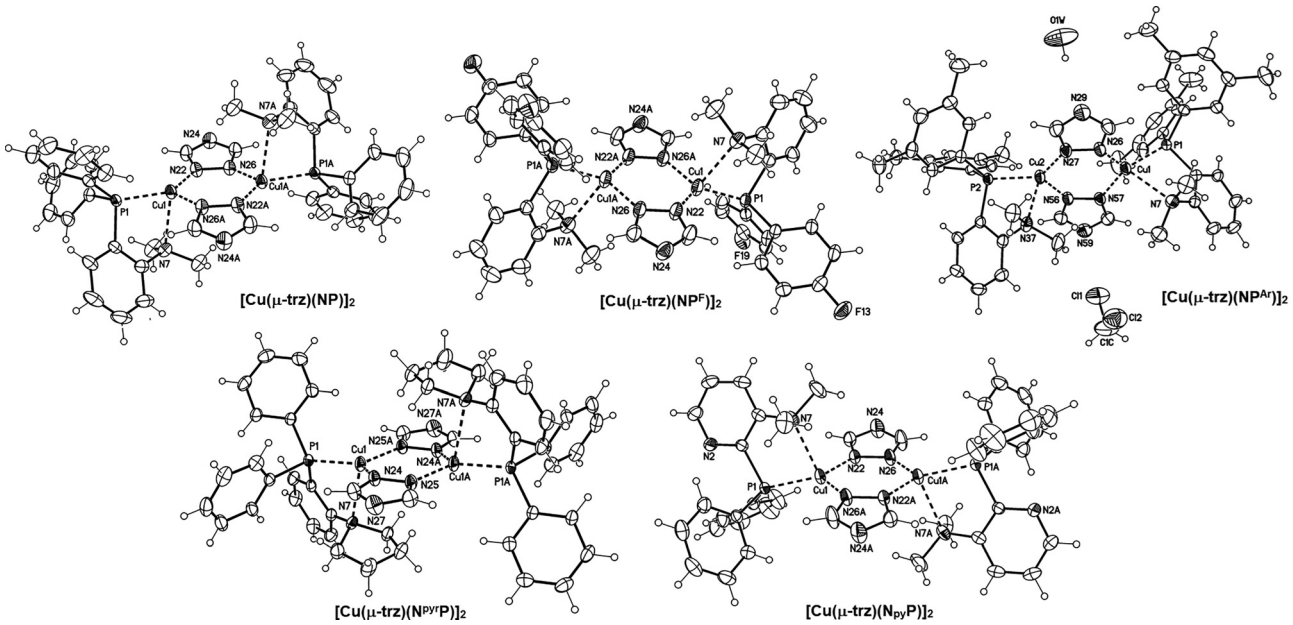

Fig. 2 X-ray structures of **[Cu(μ-trz)(NP)]$_2$**, **[Cu(μ-trz)(NP^F)]$_2$**, **[Cu(μ-trz)(NP^{Ar})]$_2$**, **[Cu(μ-trz)(N^{pyr}P)]$_2$**, and **[Cu(μ-trz)(N$_{py}$P)]$_2$**. Displacement parameters drawn at 30% probability level.

Intra- and intermolecular hydrogen bonds are in this case expected, being the distances H15···N2 and H5···N24 of 2.62 and 2.65 Å, respectively. The related H-bond parameters in complex **[Cu(μ-trz)(N$_{py}$P)]$_2$** are summarized in Table S7 (ESI†).

Photophysical properties

The UV-vis spectra in DCM of all the Cu(I) complexes are collected in Fig. 3 and are characterized by absorptions below 400 nm. No band associated with the MLCT transition in the visible range could be detected in line with the pale colour of the Cu(I) complexes as powder samples. The only observable band has maximum molar coefficients ε below 25 000 L mol^{-1} cm^{-1} and can be ascribed to the $\pi \rightarrow \pi^*$ of the coordinated phenyl fragments. This band is shifted more towards 300 nm for **[Cu(μ-trz)(NP)]$_2$** and **[Cu(μ-trz)(N$_{py}$P)]$_2$** (see black and blue lines in Fig. 3).

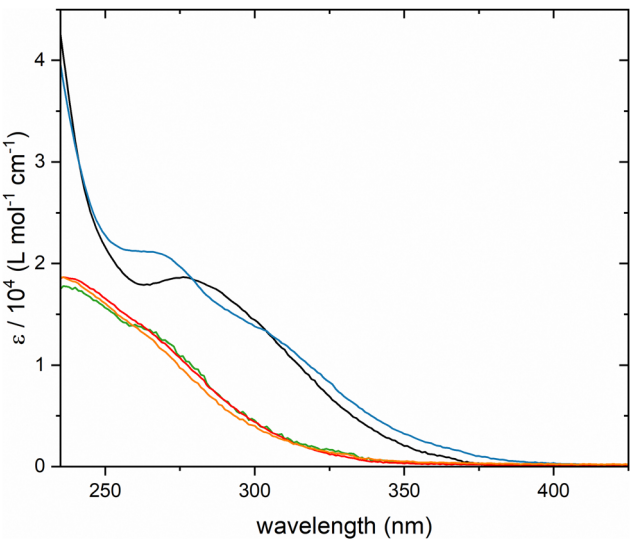

Fig. 3 UV-vis spectra collected in DCM at room temperature of **[Cu(μ-trz)(NP)]$_2$** (black line), **[Cu(μ-trz)(NP^F)]$_2$** (orange line), **[Cu(μ-trz)(NP^{Ar})]$_2$** (green line), **[Cu(μ-trz)(N^{pyr}P)]$_2$** (red line) and **[Cu(μ-trz)(N$_{py}$P)]$_2$** (blue line).

Photoluminescent measurements were carried out on powder samples and in a 1 wt% doped PMMA matrix (see Experimental section for details on the sample preparation). After exciting the Cu(I) complexes with wavelengths between 330 and 380 nm, appreciable emissions in the 480–570 nm range were observed.

The broad and featureless properties suggest the involvement of charge transfer mechanisms in the emission (see Fig. 4 for the emission spectra at 297 and 77 K both in the solid sample and PMMA matrix). It is worth mentioning that, in some of the PL spectra collected in PMMA matrix both at 297 and 77 K, a band in the 400–475 nm range was detected, as observable for instance in Fig. 4 for **[Cu(μ-trz)(NP)]$_2$**, **[Cu(μ-trz)(N^{pyr}P)]$_2$** and **[Cu(μ-trz)(N$_{py}$P)]$_2$**. This band is not due to the emission of the Cu(I) derivatives, but to a minor impurity originating during the polymerization process of PMMA. The complete photoluminescence data is provided in Table 1, and the excitation and emission spectra at different temperatures and in different matrices are collected in Fig. S2–S5 (ESI†). Compared to the Cu(I) iodo-complexes reported by Yersin *et al.* in combination with **NP** and **N^{pyr}P**,[7] the emission maxima appear to be more red-shifted passing from around 465 nm to 480 and 499 nm for **[Cu(μ-trz)(NP)]$_2$** and **[Cu(μ-trz)(N^{pyr}P)]$_2$**, respectively. The introduction of substituents in the phenyl rings of the NP ligand determined a bathochromic shift in the emission spectra in the 20–40 nm range in **[Cu(μ-trz)(NP^F)]$_2$** and **[Cu(μ-trz)(NP^{Ar})]$_2$**. As previously observed for similar compounds,[20–24] the introduction of the pyridine fragment in

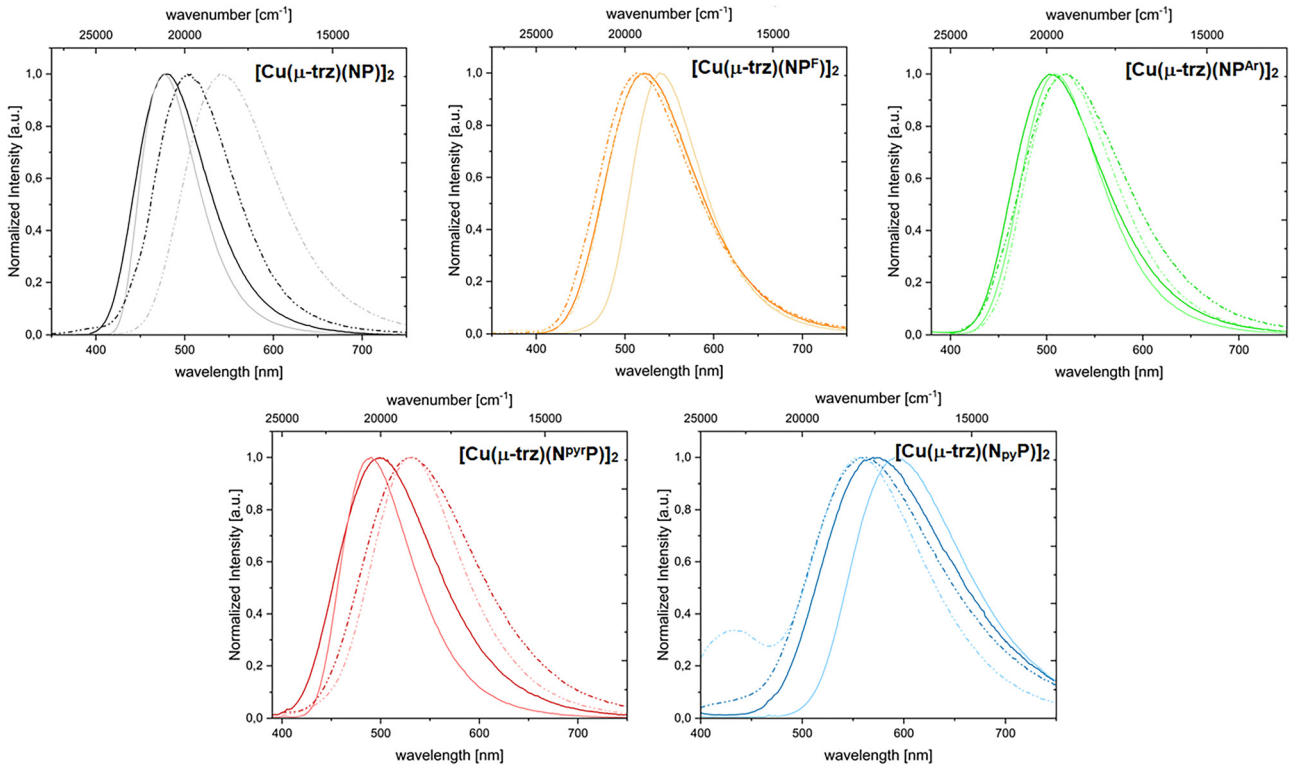

Fig. 4 Emission spectra of **[Cu(μ-trz)(NP)]$_2$** (black), **[Cu(μ-trz)(NP^F)]$_2$** (orange), **[Cu(μ-trz)(NP^{Ar})]$_2$** (green), **[Cu(μ-trz)(N^{pyr}P)]$_2$** (red) and **[Cu(μ-trz)(N$_{py}$P)]$_2$** (blue) in the solid state (solid lines) and PMMA matrix (dashed lines). Vivid and fainted colours refer to the data collected at 297 K and 77 K respectively.

Table 1 Photoluminescent data collected in the solid state and PMMA matrix at 297 and 77 K (see Experimental part for details)

	Medium	T [K]	λ_{max} [nm]	$\tau_{\langle amp \rangle}$ [μs]	ϕ	k_r [s^{-1}]
[Cu(μ-trz)(NP)]$_2$	Solid	297	480	6.7	0.25	3.73×10^4
		77	476	188.2	—	—
	PMMA	297	480	5.4	0.11	2.03×0^4
		77	539	251.3	0.24	9.56×10^1
[Cu(μ-trz)(NP^F)]$_2$	Solid	297	522	9.4	0.33	3.51×10^4
		77	539	252.0	—	—
	PMMA	297	513	4.9	0.10	2.04×10^4
		77	523	235.5	0.12	5.10×10^1
[Cu(μ-trz)(NP^{Ar})]$_2$	Solid	297	503	7.4	0.42	5.71×10^4
		77	509	218.0	—	—
	PMMA	297	521	5.3	0.20	3.75×10^4
		77	520	242.3	0.37	1.53×10^2
[Cu(μ-trz)(N^{pyr}P)]$_2$	Solid	297	499	4.4	0.16	3.64×10^4
		77	491	179.2	—	—
	PMMA	297	532	6.4	0.10	1.56×10^4
		77	530	307.5	0.14	4.55×10^1
[Cu(μ-trz)(N$_{py}$P)]$_2$	Solid	297	570	2.3	0.06	2.61×10^4
		77	591	120.9	—	—
	PMMA	297	563	2.0	0.02	1.02×10^4
		77	558	131.3	0.05	3.81×10^1

the skeleton of the NP ligand provoked the most significant red-shift of the emission maxima, reaching the yellow region with λ_{em} = 570 nm.

Although a bathochromic shift in the emission maximum due to the stabilization of a low-lying triplet state at low temperatures is a common qualitative hint for TADF materials,[6,27] for the Cu(I) complexes here investigated it was observed only for **[Cu(μ-trz)(NP^F)]$_2$**, **[Cu(μ-trz)(NP^{Ar})]$_2$** and **[Cu(μ-trz)(N$_{py}$P)]$_2$**. For the other Cu(I) complexes the opposite trend was detected.In general, for all the other Cu(I) species investigated, a hypsochromic shift of the excitation spectrum was noticeable due to the stabilization of the polar ground state once the complexes were embedded in the PMMA matrix.

As observable in Fig. 5, in the case of **[Cu(μ-trz)(N$_{py}$P)]$_2$** an additional excitation band at lower energy was detected around 390 nm, which disappeared in the PMMA matrix. Despite the nature of this band not being fully understood, we can assume that it is due to the direct $S_0 \rightarrow T_1$ transition since it is observable only in the solid state, when the high concentration of the molecules enables the detections of transitions which are normally forbidden.[28] This hypothesis is further supported by the absence of this excitation band in the PMMA matrix.

As concerns the lifetimes τ, all the Cu(I) derivatives exhibit a lifetime between 2 and 9 μs at room temperature (see Table 1). Except for **[Cu(μ-trz)(N^{pyr}P)]$_2$**, the estimated lifetime is normally shorter once the Cu(I) complexes are embedded in the polymeric matrix. The lifetime is significantly increased in the range of hundreds of μs at 77 K, as expected for TADF materials due to the freezing of the prompt fluorescence.[6,27,29] The emission decays both at the solid state and in 1 wt% PMMA at different temperatures are provided in Fig. S6–S15 (ESI†).

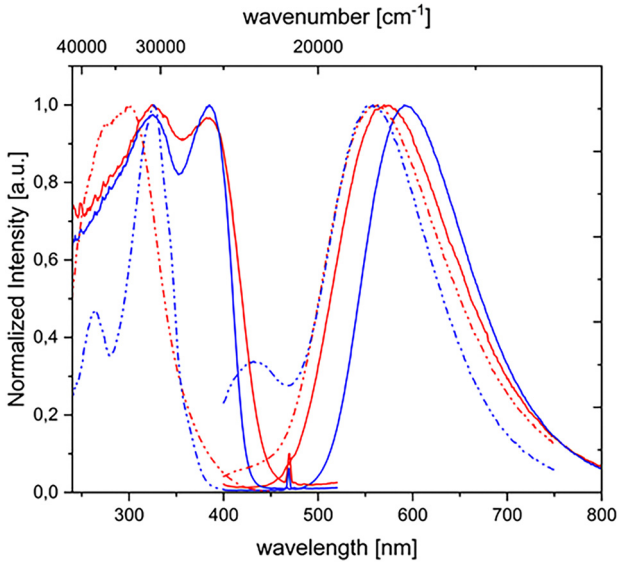

Fig. 5 Excitation and emission spectra of **[Cu(μ-trz)(N$_{py}$P)]$_2$** in the solid state (solid lines) and in the PMMA matrix (dashed lines) at room temperature (red) and 77 K (blue).

Since the emission decay curves were not monoexponential, the preexponential *B*-factors and the related lifetimes τ are collected in Table S8 (ESI†).

The photoluminescent quantum yields Φ were measured for all the Cu(I) derivatives in the solid state at 297 K and in a 1 wt% PMMA matrix both at 297 and 77 K (see Table 1). As observed also for the lifetimes, a general decrease of Φ was detected after the embedding in PMMA at room temperature. In all cases, **[Cu(μ-trz)(NP^{Ar})]$_2$** exhibited the highest values, being Φ = 0.42 at the solid state, Φ = 0.20 and Φ = 0.37 in 1 wt% PMMA at 297 K and 77 K, respectively. The radiative rate constant k_r was estimated based on the equation $\Phi = k_r/(k_r + k_{nr})$.[8,30] The comparison between the values at 297 and 77 K indicates the involvement of fluorescence ($k_r \approx 10^4$ s^{-1}) and phosphorescence ($k_r \approx 10^1$–10^2 s^{-1}) channels, supporting the TADF mechanism.

DFT calculations

The singlet ground state S_0 was optimized starting from the crystal structures of the Cu(I) derivatives, and the corresponding structures are collected in Fig. S16 (ESI†). The cutting angles θ and ϕ highlighted in Fig. S17 (ESI†) were used to compare the optimized S_0 states with the crystal structures (see Table S9, ESI†).

The computed UV-vis spectra of the Cu(I) complexes are presented in Fig. S18 (ESI†) and indicate only a minor influence of the substituents on the skeleton of the NP-ligand. For all the complexes the UV-vis spectra are characterized by a main band around 260 nm and a small shoulder at 285 nm. In contrast, for **[Cu(μ-trz)(N$_{py}$P)]$_2$** both bands are red-shifted by about 10 nm to 15 nm, as also observed in the experimental UV-vis spectrum (see Fig. 3 for comparison).

To evaluate the suitability of investigating Cu(I) complexes as TADF emitters, the first S_1 state with MLCT character (S_1^{MLCT}) was determined starting from S_0, whereas the T_1 state with MLCT character (T_1^{MLCT}) was determined from S_1^{MLCT}. As highlighted in Table S9 (ESI†), there is a change in the plane intersection angle θ of 4° to 7° for the excited states compared to the S_0 states. The bond intersection angle ϕ shows even a much stronger change, increasing from 5° to 9° for the S_0 states to 25° to 30° for the excited states. The described MLCT character is similar for all the described Cu(I) complexes, and it is illustrated in the non-relaxed difference densities in Fig. S19 (ESI†). This is because the fluorine and aryl substituents are not directly involved in the excitation, in contrast to the pyridinic nitrogen of **[Cu(μ-trz)(N$_{py}$P)]$_2$**.

The similarity of the excitations for S_1^{MLCT} and T_1^{MLCT} is also supported by the analysis of the natural orbitals. As observable in Tables S10 and S13 (ESI†), for the T_1^{MLCT} of **[Cu(μ-trz)(NP)]$_2$** the contribution of $C_{(6)}$ is 0.06 and for N_{py} in **[Cu(μ-trz)(N$_{py}$P)]$_2$** it is 0.10. For S_1^{MLCT} the influence is even weaker with 0.06 for $C_{(6)}$ and 0.07 for N_{py}. The natural population analysis of **[Cu(μ-trz)(NP^{F})]$_2$** and **[Cu(μ-trz)(NP^{Ar})]$_2$** are similar to the other two complexes (see Tables S11 and S12 for completeness, ESI†).

To determine the amount of charge transfer, the overlap between the natural transition orbitals S_{NTO} was calculated and the data is provided in Table S14 (ESI†). The NTOs show the same character as the non-relaxed difference densities illustrated in Fig. S19 (ESI†). The S_{NTO} analysis indicates that **[Cu(μ-trz)(N$_{py}$P)]$_2$** has a slightly higher charge transfer character for T_1^{MLCT} and S_1^{MLCT} compared to the other Cu(I) complexes. The lower S_{NTO} is also reflected in the calculated ΔE_{ST}^{adia}, which is 179 meV for **[Cu(μ-trz)(N$_{py}$P)]$_2$** and between 234 and 242 meV for the other Cu(I) complexes. These values are in a reasonable range for TADF.[6]

As observable in Table S15 (ESI†), HOMO → LUMO and HOMO−1 → LUMO+1 are the dominant excitation contributions, being the HOMO and HOMO−1 as well as the LUMO and LUMO+1 nearly degenerate due to symmetry.

A similar trend was observed in the transition dipole moment μ_T for the excited states, where **[Cu(μ-trz)(N$_{py}$P)]$_2$** has both the lowest S_{NTO} and the lowest μ_T (see Table S14, ESI†). This suggests a lower radiation rate for **[Cu(μ-trz)(N$_{py}$P)]$_2$** compared to the other Cu(I) derivatives, as supported also by the experimental data (see Table 1).[31]

It should be noted that an additional T_1 state with ligand-centred (LC) character was found in all the Cu(I) complexes, as illustrated in Fig. 6 and Fig. S20 (ESI†). An S_1 state with LC character could not be determined starting from T_1^{LC}. Instead, the optimization terminated again in S_1^{MLCT}, and T_1^{LC} was obtained from the S_0 state. As highlighted in Table S16 (ESI†), due to the local character of the excitation for T_1^{LC}, S_{NTO} is larger compared to T_1^{MLCT}, which is also energetically higher compared to the former (12 *vs.* 19 kJ mol^{-1}). The local character in T_1^{LC} probably results from the increased distance between the Cu atom and the nitrogen atom of the ligand, d(Cu···N$_L$). However, T_1^{MLCT} is occupied despite the increased energy enabling the TADF mechanism probably due to environmental effects, which led to a stabilization and made it more energetically favourable compared to T_1^{LC}.

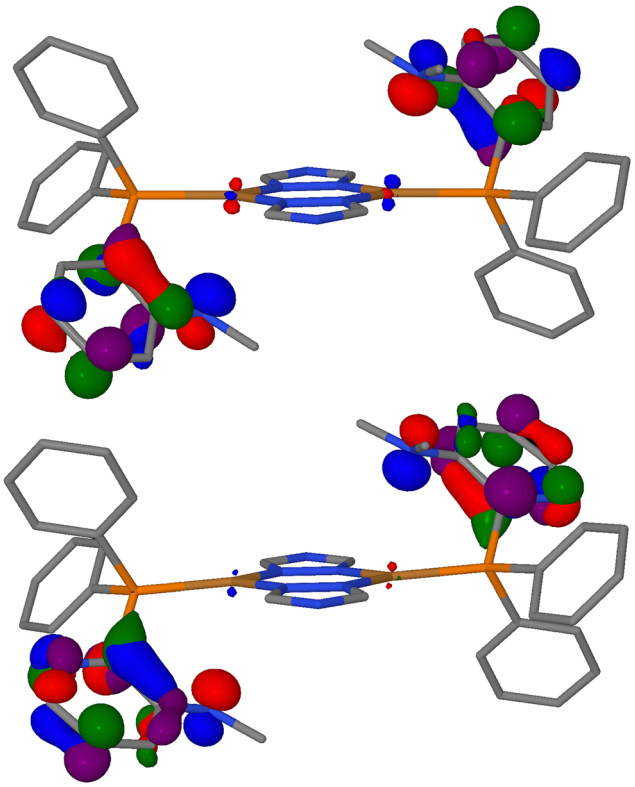

Fig. 6 NTOs of the lowest excitation at the T_1 state with LC character for **[Cu(μ-trz)(NP)]$_2$** (top) and **[Cu(μ-trz)(N$_{py}$P)]$_2$** (bottom), where blue/red stands for a loss in electron density and green/purple for an increase in electron density (isovalue = $\pm 0.06 a_0^{-3/2}$; TDA-CAM-B3LYP/SVPD; hydrogen atoms are omitted for clarity).

Experimental

Materials and methods

The solvents were purchased from Fisher, if not stated otherwise. Dichloromethane, toluene and THF were dried with the solvent purification system (SPS) from MBraun (model MB-SPS-800) and degassed with argon before usage. Dry DMF and *N*,*N*-dimethylacetamide (DMAC) were purchased from Acros Organics, whereas *n*-pentane or diethyl ether employed for the precipitation of the Cu(I) complexes were acquired from Merck. CuCl pellets, ^{t}BuOK, methyl iodide, 1,4-dibromobutane, *N*,*N*-diisopropylethylamine (DIPEA), sodium hydride (60% in mineral oil), *n*-butyllithium (2.5 M in hexane), palladium(II) acetate, diphenylphosphine and all the chloro(diaryl)phosphine were purchased from Merck. 2-Bromoaniline was purchased from chemPUR, while 3-amino-2-bromopyridine and 1,2,4-triazole were obtained respectively from BLDPharm and abcr. All chemicals were used without any further purification. The heteronuclear NMR spectra of the Cu(I) complexes were recorded in $CDCl_3$ purchased from Eurisotop. All reactions were carried out using Schlenk techniques under Ar atmosphere.

General information concerning NMR, mass spectrometry, IR and elemental analyses, and melting points is detailed in the ESI.† Additional information on the experimental procedure is available *via* the Chemotion Repository.[32]

Crystal structure determination

Single-crystal X-ray diffraction was carried out on a Bruker D8 Venture diffractometer with a Photon^{II} detector at 298(2) K using Cu-Kα radiation (λ = 1.54178 Å). Dual space methods SHELXT were used for the structure solution and the refinement was carried out using SHELXL-2014 (full-matrix least-squares on F^2).[33,34] The hydrogen atoms were refined using a riding model (H(O) free). Semi-empirical absorption corrections were applied. For **[Cu(μ-trz)(NP^{Ar})]$_2$** an extinction correction was applied. In **[Cu(μ-trz)(NP^{F})]$_2$** disordered water molecules were squeezed out (see cif-files for details).[35,36]

CCDC 2380060–2380064 contain the ESI† crystallographic data for this paper.

Photoluminescent measurements

The UV-vis spectra were collected in dichloromethane solutions employing an Analytik Jena Specord 50 instrument. All the solid-state photophysical measurements were performed under rigorous exclusion of air and moisture. The dichloromethane (DCM) used for steady-state absorption spectroscopy was dried and degassed prior to the measurement. Polymethylmethacrylate (PMMA) films were prepared by drop casting method with 1 wt% of complexes dissolved in DCM, followed by evaporation of the solvent and drying of polymeric films under high vacuum. Excitation and emission spectra were recorded on an Edinburgh Instrument FLSP920 or FLS1000 spectrometer, equipped with a 450 W Xenon arc lamp. The emission was collected at right angle to the excitation source with the emission wavelength selected using a double-grated monochromator for the excitation and emission pathways and detected by a red-sensitive photomultiplier (PMT-R928 or 980) as detector. The excitation and emission spectra were corrected using the standard corrections supplied by the manufacturer for the spectral power of the excitation source and the sensitivity of the detector. Quantum yields of polymeric matrices were measured using an integrating cryosphere (Microstat N2) from Oxford Instruments. Alternatively, quantum yields of the solid samples were recorded using a quantaurus-QY absolute PL quantum yield spectrometer C11347 by Hamamatsu. The luminescence lifetimes were measured using a VPLED 320/380 nm, with 1 to 5 μs pulse width and an MCS module, depending on the time range.

DFT calculations

All calculations were carried out with Turbomole[37] and the resolution of identity approximation using symmetry.[38] CAM-B3LYP was employed as functional.[39] For Cu, P, N, and the carbon atoms in the triazoles the def2-SVPD basis was used, whereas for the remaining atoms, def2-SVP was employed. This combination is abbreviated as SVPD. The numerical integration for the calculation of the energy was carried out with the lattice of size four.[40] C_i symmetry for **[Cu(μ-trz)(NP)]$_2$**, **[Cu(μ-trz)(NP^{F})]$_2$** and **[Cu(μ-trz)(N$_{py}$P)]$_2$**, and C_s symmetry for **[Cu(μ-trz)(NP^{Ar})]$_2$** were respectively utilized. Weight derivatives were accounted for during the optimizations[41] and the structures were converged when the change in energy was below $10^{-7} E_h$ and the change in the cartesian gradients was below $10^{-5} E_h/a_0$. The singlet ground state

(S_0) optimizations were started from the crystal structure. The Tamm–Dancoff approximation (TDA) within time-dependent DFT (TD-DFT)[42] was used starting from S_0 to obtain the first singlet excited state S_1 with metal-to-ligand charge transfer (MLCT) character, and the first triplet excited state T_1 with ligand-centred (LC) character. The T_1 with MLCT character was obtained with the respective S_1 as the starting point. The singlet–triplet energy gap (ΔE_{ST}^{adia}) was calculated as the difference in electronic energy of S_1 and T_1 with MLCT character. For the computed UV-vis spectra Gaussian broadening (FWHM = 2500 cm^{-1}) and oscillator strengths in length representation were used.

Conclusions

1,2,4-Triazole was successfully employed as bridging ligand for the preparation of blue- to yellow-emitting Cu(I) dimeric complexes having aminophosphanes as chelating NP-ligands. The molecular structure of the Cu(I) complexes was unambiguously confirmed through single-crystal X-ray diffraction. The photoluminescence data conducted at room temperature and 77 K in the solid state and in a 1 wt% doped PMMA matrix support the TADF mechanism due to the appreciable increase in the observed lifetime τ and the presence of two significantly different radiative rate constants k_r at 297 and 77 K.

From a computational point of view, the excited states with MLCT characters are structurally very similar to each other, and these similarities could be observed also by analysing the natural transition orbitals (NTOs). For the Cu(I) complexes investigated, all these aspects lead to a ΔE_{ST}^{adia} in the 179–242 meV range, with the complex with the lowest ΔE_{ST}^{adia} also showing the lowest transition dipole moment μ_T for the related excited states.

To conclude, the experimental and computed data here presented support that the emission properties are due to TADF. However, compared to the similar Cu(I) complexes with NP-ligands, the absence of halides in the coordination sphere significantly enhances the solubility of these compounds in common organic solvents without significantly affecting the photoluminescent properties, thus making them suitable candidates to be applied in solution-processed OLEDs.

Author contributions

Valentina Ferraro: data curation, formal analysis, investigation, methodology, validation, writing – original draft, writing – review & editing. Xuemin Gan: conceptualization, investigation, methodology. Florian R. Rehak: formal analysis, investigation, methodology, writing – original draft. Philipp Ralle: formal analysis, investigation, methodology, writing – original draft, writing – review & editing. Martin Nieger: data curation, formal analysis, investigation, methodology, validation, writing – original draft, writing – review & editing. Andreas Steffen: funding acquisition, validation, writing – original draft, writing – review & editing. Wim Klopper: funding acquisition, validation, writing – original draft, writing – review & editing. Stefan Bräse: funding acquisition, validation, writing – original draft, writing – review & editing.

Data availability

The details on the chemical synthesis and original analytical data were added to the repository Chemotion **https://www.chemotion.net/home**.[32]

Conflicts of interest

There are no conflicts to declare.

Acknowledgements

X. G. acknowledges the support provided by the China Scholarship Council and V. F. thanks Luca Schichtel for performing some of the experimental procedures. The authors thank the Karlsruhe School of Optics and Photonics (KSOP) and the DFG for financial support through Germany's Excellence Strategy 3D Matter Made to Order (3DMM2O, Grant No. EXC-2082/1-390761711).

Notes and references

1 J. G. Haasnoot, *Coord. Chem. Rev.*, 2000, **200–202**, 131–185.
2 L. Bergmann, C. Braun, M. Nieger and S. Bräse, *Dalton Trans.*, 2018, **47**, 608–621.
3 M. Freund, *Ber. Dtsch. Chem. Ges.*, 2006, **29**, 2483.
4 X.-L. Chen, R. Yu, X.-Y. Wu, D. Liang, J.-H. Jia and C.-Z. Lu, *Chem. Commun.*, 2016, **52**, 6288–6291.
5 C. E. Housecroft and E. C. Constable, *J. Mater. Chem. C*, 2022, **10**, 4456–4482.
6 V. Ferraro, C. Bizzarri and S. Brase, *Adv. Sci.*, 2024, **11**, 2404866.
7 M. J. Leitl, F. R. Kuchle, H. A. Mayer, L. Wesemann and H. Yersin, *J. Phys. Chem. A*, 2013, **117**, 11823–11836.
8 H. Yersin, *Highly Efficient OLEDs: Materials Based on Thermally Activated Delayed Fluorescence*, Wiley-VCH, 2019.
9 S. B. Harkins and J. C. Peters, *J. Am. Chem. Soc.*, 2005, **127**, 2030–2031.
10 M. Klein, N. Rau, M. Wende, J. Sundermeyer, G. Cheng, C.-M. Che, A. Schinabeck and H. Yersin, *Chem. Mater.*, 2020, **32**, 10365–10382.
11 J.-H. Jia, X.-L. Chen, J.-Z. Liao, D. Liang, M.-X. Yang, R. Yu and C.-Z. Lu, *Dalton Trans.*, 2019, **48**, 1418–1426.
12 T. Hofbeck, T. A. Niehaus, M. Fleck, U. Monkowius and H. Yersin, *Molecules*, 2021, **26**, 3415.
13 A. Schinabeck, M. J. Leitl and H. Yersin, *J. Phys. Chem. Lett.*, 2018, **9**, 2848–2856.
14 T. Hofbeck, U. Monkowius and H. Yersin, *J. Am. Chem. Soc.*, 2015, **137**, 399–404.
15 A. V. Artem'ev, M. P. Davydova, A. S. Berezin, M. R. Ryzhikov and D. G. Samsonenko, *Inorg. Chem.*, 2020, **59**, 10699–10706.
16 M. P. Davydova, A. S. Berezin, D. G. Samsonenko and A. V. Artem'ev, *Inorg. Chim. Acta*, 2021, **521**, 120347.
17 A. Kobayashi, T. Hasegawa, M. Yoshida and M. Kato, *Inorg. Chem.*, 2016, **55**, 1978–1985.
18 A. Y. Baranov, A. S. Berezin, D. G. Samsonenko, A. S. Mazur, P. M. Tolstoy, V. F. Plyusnin, I. E. Kolesnikov and A. V. Artem'ev, *Dalton Trans.*, 2020, **49**, 3155–3163.

19 B. Goswami, T. J. Feuerstein, R. Yadav, S. Lebedkin, P. J. Boden, S. T. Steiger, G. Niedner-Schatteburg, M. Gerhards, M. M. Kappes and P. W. Roesky, *Chem. – Eur. J.*, 2021, **27**, 15110–15119.
20 D. M. Zink, M. Bachle, T. Baumann, M. Nieger, M. Kuhn, C. Wang, W. Klopper, U. Monkowius, T. Hofbeck, H. Yersin and S. Brase, *Inorg. Chem.*, 2013, **52**, 2292–2305.
21 D. M. Zink, D. Volz, T. Baumann, M. Mydlak, H. Flügge, J. Friedrichs, M. Nieger and S. Bräse, *Chem. Mater.*, 2013, **25**, 4471–4486.
22 L. Bergmann, G. J. Hedley, T. Baumann, S. Bräse and I. D. W. Samuel, *Sci. Adv.*, 2016, **2**, e1500889.
23 J. M. Busch, D. M. Zink, P. Di Martino-Fumo, F. R. Rehak, P. Boden, S. Steiger, O. Fuhr, M. Nieger, W. Klopper, M. Gerhards and S. Bräse, *Dalton Trans.*, 2019, **48**, 15687–15698.
24 J. M. Busch, D. S. Koshelev, A. A. Vashchenko, O. Fuhr, M. Nieger, V. V. Utochnikova and S. Bräse, *Inorg. Chem.*, 2021, **60**, 2315–2332.
25 J. M. Busch, F. R. Rehak, V. Ferraro, M. Nieger, M. Kemell, O. Fuhr, W. Klopper and S. Bräse, *ACS Omega*, 2024, **9**, 2220–2233.
26 N. V. S. Harisomayajula, S. Makovetskyi and Y.-C. Tsai, *Chem. – Eur. J.*, 2019, **25**, 8936–8954.
27 G. U. Mahoro, J. Fernandez-Cestau, J. L. Renaud, P. B. Coto, R. D. Costa and S. Gaillard, *Adv. Opt. Mater.*, 2020, **8**, 2000260.
28 M. Gernert, U. Müller, M. Haehnel, J. Pflaum and A. Steffen, *Chem. – Eur. J.*, 2017, **23**, 2206–2216.
29 A. Steffen and B. Hupp, *Comprehensive Coordination Chemistry III*, Elsevier, 2021, pp. 466–502.
30 H. Yersin, A. F. Rausch, R. Czerwieniec, T. Hofbeck and T. Fischer, *Coord. Chem. Rev.*, 2011, **255**, 2622–2652.
31 H. Yersin, R. Czerwieniec, M. Z. Shafikov and A. F. Suleymanova, *ChemPhysChem*, 2017, **18**, 3508–3535.
32 V. Ferraro, X. Gan and S. Bräse, *Chemotion Repository*, 2024, DOI: **10.14272/collection/VF_2024-03-21**.
33 G. M. Sheldrick, *Acta Crystallogr., Sect. A: Found. Adv.*, 2015, **71**, 3–8.
34 G. M. Sheldrick, *Acta Crystallogr., Sect. C: Struct. Chem.*, 2015, **71**, 3–8.
35 A. L. Spek, *Acta Crystallogr., Sect. D: Biol. Crystallogr.*, 2009, **65**, 148–155.
36 A. L. Spek, *Acta Crystallogr., Sect. C: Struct. Chem.*, 2015, **71**, 9–18.
37 *TURBOMOLE V7.5 2020: a development of University of Karlsruhe and Forschungszentrum Karlsruhe GmbH*, Turbomole GmbH, 2007. **https://www.turbomole.org**.
38 R. A. Kendall and H. A. Früchtl, *Theor. Chem. Acc.*, 1997, **97**, 158–163.
39 T. Yanai, D. P. Tew and N. C. Handy, *Chem. Phys. Lett.*, 2004, **393**, 51–57.
40 O. Treutler and R. Ahlrichs, *J. Chem. Phys.*, 1995, **102**, 346–352.
41 P. Deglmann, F. Furche and R. Ahlrichs, *Chem. Phys. Lett.*, 2002, **362**, 511–518.
42 S. Hirata and M. Head-Gordon, *Chem. Phys. Lett.*, 1999, **314**, 291–299.